GFZ
Helmholtz-Zentrum
POTSDAM

Originally published as:

Dobslaw, H., Dill, R., Grötzsch, A., Brzezinski, A., Thomas, M. (2010): Seasonal polar motion excitation from numerical models of atmosphere, ocean, and continental hydrosphere. - Journal of Geophysical Research, 115, B10406

DOI: 10.1029/2009JB007127

Seasonal polar motion excitation from numerical models of atmosphere, ocean, and continental hydrosphere

H. Dobslaw,[1] R. Dill,[1] A. Grötzsch,[1] A. Brzeziński,[2,3] and M. Thomas[1]

Received 17 November 2009; revised 21 June 2010; accepted 8 July 2010; published 8 October 2010.

[1] Effective angular momentum functions from atmosphere, oceans, and terrestrial water storage are obtained from European Centre for Medium-Range Weather Forecasts atmospheric data and corresponding simulations with the Ocean Model for Circulation and Tides and the Land Surface and Discharge Model (LSDM). Mass exchanges among the subsystems are realized by means of freshwater fluxes, causing the total ocean mass to vary predominantly annually. Variations in total ocean mass affect the oceanic excitations of the annual wobble by almost 1 milliarc second (mas) for both prograde and retrograde components, whereas the motion term contributions of terrestrial water flow derived from LSDM are found to be 3 orders of magnitude smaller. Since differences to geodetic excitations are not substantially reduced and regional decompositions demonstrate the large spatial variability of contributions to seasonal polar motion excitation that compensate each other when integrated globally, it is concluded that the closure of the seasonal excitation budget is still inhibited by remaining model errors in all subsystems.

Citation: Dobslaw, H., R. Dill, A. Grötzsch, A. Brzeziński, and M. Thomas (2010), Seasonal polar motion excitation from numerical models of atmosphere, ocean, and continental hydrosphere, *J. Geophys. Res.*, *115*, B10406, doi:10.1029/2009JB007127.

1. Introduction

[2] The rotation of the Earth is not uniform in time but varies due to both external torques and internal processes that alter its mass distribution. While external torques cause the Earth to precess and nutate, internal excitation processes are responsible for a wobbling of the Earth as it rotates. These wobbling motions consist of a few discrete frequencies that entirely depend on the Earth's density and elasticity structure, i.e., the free wobbles, as well as a broad frequency band in response to various forcing mechanisms, which are known as forced wobbles. Among these, wobbling motions on the annual period and its higher harmonics linked to the seasons are particularly apparent.

[3] The different wobbles of the Earth can be determined by analyzing observations of the intermediate rotational pole of the Earth in the terrestrial reference frame, which is precisely observed by space geodetic techniques. The accuracy of its daily position reaches 0.05 milliarc second (mas) [*Bizouard and Seoane*, 2010], which corresponds to a horizontal displacement of 1.5 mm on the Earth's surface. Although highly precise, the observations themselves only provide globally integrated signals that do not contain further information to separate the contributions from different components of the Earth's system. Complementary observations and numerical models are therefore required to relate these signals to individual processes acting on such different subsystems like atmosphere, ocean, continental hydrosphere, and the fluid core.

[4] By means of numerical models, various geophysical processes have been shown to contribute to the excitation of the forced wobbles. This includes the presence of high pressure systems over continental landmasses during winter time [*Barnes et al.*, 1983], and corresponding variations in atmospheric wind systems [*Rosen and Salstein*, 1983]. Variations in ocean bottom pressure and currents have been shown to contribute substantially [*Ponte et al.*, 1998], and terrestrial water storage variations have been identified to contribute in particular to the excitation of the annual wobble [*Kuehne and Wilson*, 1991]. Although numerical models are steadily improving and have allowed more detailed insights into the contributions of individual subsystems [*Gross et al.*, 2003; *Chen and Wilson*, 2005] including the evaluation of regional contributions [*Nastula et al.*, 2009], the excitation budget is still not balanced even for the annual period. This has been related to both model insufficiencies and to a lack of mass consistency among the individual models of the subsystems considered [*Brzeziński et al.*, 2009].

[5] In this study, geophysical excitations of the annual wobble and its higher harmonics, i.e., the seasonal wobbles, are revisited by means of model output from different global data sets of the European Centre for Medium-Range

[1]Section 1.3: Earth System Modeling, Deutsches GeoForschungsZentrum, Potsdam, Germany.
[2]Faculty of Geodesy and Cartography, Warsaw University of Technology, Warsaw, Poland.
[3]Space Research Centre, Polish Academy of Sciences, Warsaw, Poland.

Copyright 2010 by the American Geophysical Union.
0148-0227/10/2009JB007127

Weather Forecasts (ECMWF). Atmospheric contributions are combined with data from the Ocean Model for Circulation and Tides (OMCT) [*Thomas*, 2002] and the Land Surface and Discharge Model (LSDM) [*Dill*, 2009], where both are consistently forced with mass, momentum, and energy fluxes from the atmosphere (section 2). The realization of mass conservation within the atmosphere-hydrosphere modeling system is described in section 3. Geophysical effective angular momentum functions calculated for all subsystems (section 4) are contrasted against geodetic excitation functions derived from observed pole coordinates in section 5. Contributions of individual latitude bands to the excitation of the seasonal wobbles are examined in section 6, followed by some concluding remarks in the final section.

2. Geophysical Fluids Data

[6] The combination of numerical models applied in this study consists of three different atmospheric data sets from the ECMWF numerical weather prediction model that provide the angular momentum budget of the atmosphere and freshwater, energy, and momentum fluxes required to force the land surface model LSDM. Ocean discharge calculated from the continental model is combined with the atmospheric forcing fields to simulate the oceanic response with the global ocean model OMCT.

2.1. ECMWF Atmospheric Data

[7] Covering more than four decades from 1957 until 2001, the ECMWF reanalysis ERA-40 [*Uppala et al.*, 2005] provides 6 hourly analysis data which are available on 23 pressure levels with 1.25° horizontal resolution. Although the reanalysis was intended to provide a homogeneous data set suitable for climate studies, spurious trends and changes in variability have been detected in various key quantities, including middle atmosphere dynamics [see, e.g., *Randel et al.*, 2009], the hydrological cycle [*Hagemann et al.*, 2005], and atmospheric mass transports [*Graversen et al.*, 2007].

[8] Substantial improvements of the physical model and the data assimilation techniques led recently to a new reanalysis effort. ERA Interim [*Uppala et al.*, 2008] has been produced since 1989 and is expected to be updated sequentially with latencies of a few months. The data used in this study is distributed on 37 pressure levels with a horizontal resolution of 1°. Compared to ERA-40, the long-term homogeneity of ERA Interim has been significantly improved. Excessive precipitation in the tropics has been largely reduced, although it still remains higher than observational estimates. The Brewer-Dobson circulation is more reasonable now, and biases in wind speed over the extra-tropical oceans are less distinct. The annual cycle of specific humidity is much smaller than in ERA-40, in particular the transports across the tropopause are reduced [*Uppala et al.*, 2008].

[9] In addition to the reanalysis data, which is typically available with latencies of months to years, operational ECWMF data is considered as well. The operational model is subject to ongoing developments intended to continuously improve the weather forecast accuracies. Upgrades of the operational model usually take place two to four times a year, including for example changes in model physics, changes in observation handling or the introduction of improved data assimilation algorithms. The current model version runs on a T799 grid (approximately 25 km horizontal resolution) with 91 vertical levels. The data is currently provided on 25 pressure levels, and a horizontal resolution of 1° is used in this study.

2.2. Land Surface Discharge Model (LSDM)

[10] The continental hydrology is simulated by the Land Surface Discharge Model (LSDM) [*Dill*, 2009]. The model simulates global water storage variations of surface water in rivers, lakes, wetlands, groundwater, and soil moisture, as well as from water stored as snow and ice. Based on the simplified Land Surface Scheme and the Hydrological Discharge Model by *Hagemann* [1998], the model is discretized on a regular 0.5° global grid and is integrated with a 24 h time step. The LSDM is forced with precipitation, evaporation, and temperature from an atmospheric model. Depending on the saturation-capacity ratio of the soil layer, water reaching the surface is divided into drainage that percolates downward into the deeper soil, and fast surface runoff. In open water areas, runoff is generated directly from precipitation and evaporation. Runoff and drainage are finally combined into river flow which is routed in subsequent time steps toward the ocean. Rivers are represented by a flow direction map that has been derived from a 1/12° global topography data set. Retention times of the water flow in each grid cell depend on the topographic gradient, the distance in flow direction, and additional parameters that take into account wetland and lake conditions [*Hagemann and Dümenil*, 1998].

2.3. Ocean Model for Circulation and Tides

[11] Ocean dynamics are simulated by means of the Ocean Model for Circulation and Tides (OMCT) [*Thomas*, 2002]. The model has been developed by adjusting the originally climatological Hamburg Ocean Primitive Equation Model [*Wolff et al.*, 1996; *Drijfhout et al.*, 1996] to the weather time scale and coupling with an ephemeral tidal model. The model is based on the nonlinear momentum balance equation, the continuity equation, and conservation equations for heat and salt. The hydrostatic and Boussinesq approximations are applied. Water elevations, three-dimensional horizontal velocities, potential temperature as well as salinity are calculated prognostically; vertical velocities are determined diagnostically from the incompressibility condition. A prognostic sea-ice model is implemented to predict thickness, compactness, and drift of ice. The ocean model uses a time step of 30 min, a constant horizontal resolution of 1.875° in latitude and longitude, and 13 vertical layers. OMCT is forced by 6 hourly wind stress, atmospheric surface pressure, 2m-temperature and freshwater flux.

3. Freshwater Fluxes and Global Mass Conservation

[12] Besides energy and momentum fluxes, mass transports, in terms of freshwater fluxes among the individual subsystems, need to be adequately described by numerical models attempting to assess the global angular momentum budget. Atmospheric freshwater fluxes are obtained from the first hours of the forecast following each ECMWF analysis. While downloaded on a regular 1° grid from the

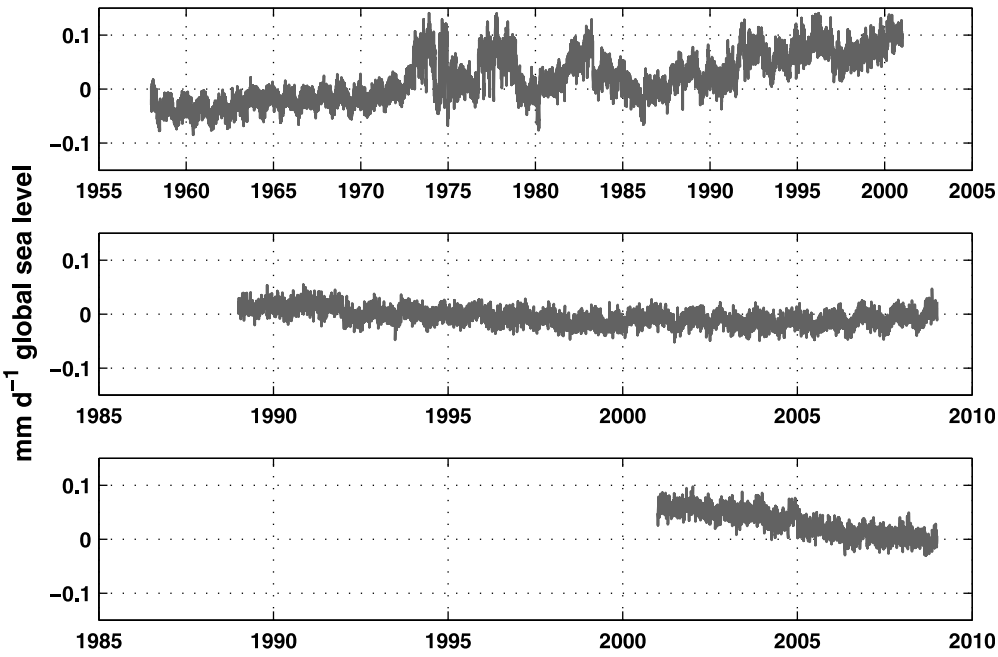

Figure 1. Net effect of globally integrated freshwater fluxes out of the atmosphere from (top) ERA-40, (middle) ERA Interim, and (bottom) operational ECMWF data expressed in terms of global mean eustatic sea level change.

ECMWF archives, the given mass flux is equally assigned to the 0.5° LSDM grid cells that fit into the 1° grid box. Proportional to the fraction of land-cover defined by LSDM, a part of the freshwater is routed into the land surface model and transported laterally away, while the remaining atmospheric freshwater is combined with the LSDM discharge estimates representing the amount of water that is finally reaching the oceans. Due to the coarser spatial resolution of OMCT and some oversized stream barriers and throughflows required for dynamical reasons, discharge is routed into the nearest ocean cell within a 4° search radius.

[13] However, atmospheric freshwater fluxes have found to be biased in both ERA-40 [*Andersson et al.*, 2005] and, to a lesser extent, in ERA Interim. Imbalances in the moisture budget imposed by the assimilation scheme cause intensified rain events during the first hours of the forecast, leading to even a net mass loss of the atmosphere over the oceans. Integrating daily freshwater fluxes over the globe indicates substantial imbalances (Figure 1). During the 1960s, evaporation typically exceeds precipitation. Subsequently, precipitation rates are strongly increased in 1973, where the first satellite observations became available. Also, volcanic eruptions like El Chichon in 1982 and the 1991 Pinatubo event clearly affect the radiance bias corrections in ERA-40, resulting in an overestimation of tropical precipitation [*Uppala et al.*, 2008]. During the 1990s, atmospheric freshwater fluxes are always positive, that would lead to an unrealistic global sea level rise of roughly 1.5 cm yr^{-1}. The mass balance improves substantially with ERA Interim, where globally integrated freshwater fluxes are almost zero during the years. However, changes in trends can be still detected around 2000, where a decelerating sea level rise is turned into a gradual decline. A comparable weak negative trend in sea level rise is visible within the operational data, where major efforts in improving the hydrological cycle took place very recently [*Andersson et al.*, 2005], bringing the atmospheric freshwater budget almost into balance around 2007.

[14] In order to mitigate the effects of long-term variations in atmospheric freshwater fluxes, a correction to the total ocean mass is implemented in OMCT by adopting the "passive ocean" concept [*Clarke et al.*, 2005]. By assuming that mass is solely redistributed among atmosphere, ocean and continental hydrosphere while tentatively neglecting glaciers and ice caps, a homogeneous layer of excess mass is added together with a technically similar correction to account for mass changes due to the Boussinesq approximation [*Greatbatch*, 1994]. Since only the total mass of the ocean is adjusted homogeneously, dynamical effects of the freshwater fluxes in both LSDM and OMCT remain unaffected.

[15] During the 1960s, surface pressure analyses of ERA-40 contain higher uncertainties, primarily due to limitations in the observational networks (Figure 2). At the same time, low precipitation rates lead to smaller amounts of water stored on land, requiring an increase in total ocean mass as modeled with OMCT. The subsequent rise in precipitation rates around 1972 leads to an increase in continental water storage and a corresponding drop in global sea level. Variations are more reasonable from 1980 onward, where total atmospheric mass estimates are getting less noisy and strong interannual variations in the total amount of continental water storage are fading out. Total ocean mass variations exhibit seasonal variations of roughly 1.5 cm peak-to-peak amplitudes, which is broadly consistent with GRACE satellite gravimetry observations [*Chambers et al.*, 2004]. Similar variations are obtained from the corresponding simulations forced by ERA Interim and the operational ECMWF data. Although substantial inter-annual differences exist, i.e., at the end of 2004 and 2007, seasonal variations

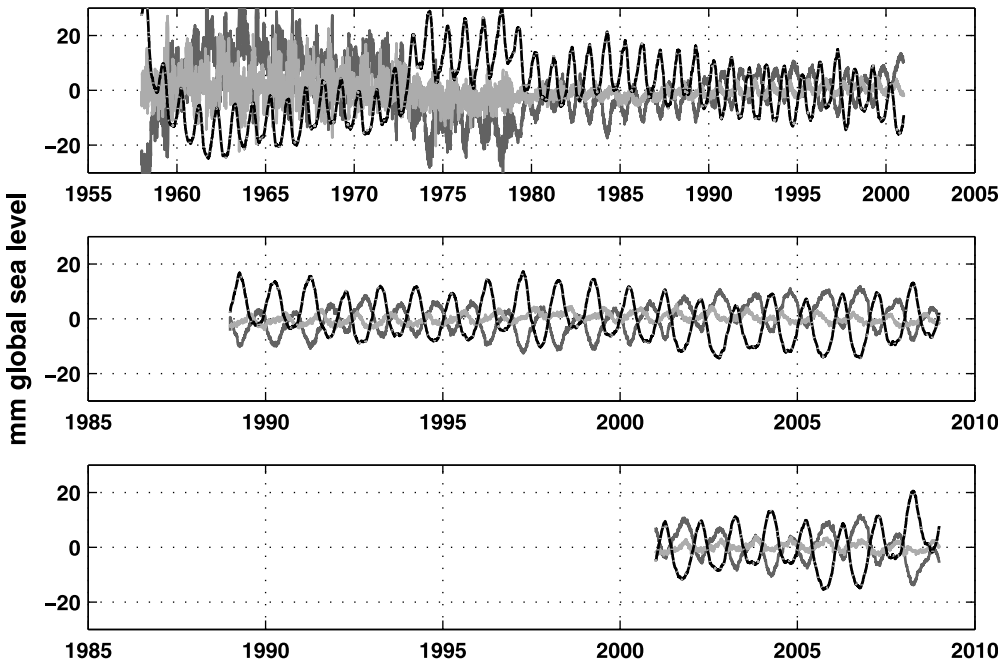

Figure 2. Variations in total water mass stored in atmosphere (solid gray), ocean (solid black), and continental water storage (solid black with white dots) derived from (top) ERA-40, (middle) ERA Interim, and (bottom) operational ECMWF data, expressed in terms of global mean eustatic sea level.

in total ocean mass are represented in all three model combinations reasonably well.

4. Geophysical EAM Functions

[16] Based on the conservation of angular momentum in the Earth's system, the orientation of the rotational axis in a mean mantle reference frame can be expressed by the Liouville equation [*Gross*, 2009]. Solving this equation by a perturbation approach describing mass displacements as small variations δI of the tensor of inertia $I = I_0 + \delta I$ together with relative angular momentum contributions h related to mass movements and keeping terms of first order, the variations in Earth rotation are described by small deviations from its mean rotational velocity Ω known as polar motion and changes in length-of-day. Contributions from dynamical processes within the geophysical fluids are summarized in terms of effective angular momentum functions χ_i (EAM) [*Barnes et al.*, 1983]

$$\chi_1 = \frac{1}{1-\frac{k_2}{k_s}} \frac{1}{\Omega^2 (C_m - A_s)} \left[(1+k_l) \cdot \Omega^2 \delta I_{13} + \Omega h_1 \right],$$

$$\chi_2 = \frac{1}{1-\frac{k_2}{k_s}} \frac{1}{\Omega^2 (C_m - A_s)} \left[(1+k_l) \cdot \Omega^2 \delta I_{23} + \Omega h_2 \right].$$

These geophysical EAM functions include the effects due to rotational deformation, where k_2 is the degree two body Love number of the Earth, and k_s the secular Love number corresponding to the fluid limit of k_2. Elastic deformations due to time-variable mass loads are taken into account by means of the second degree load Love number k_l. Core motion is decoupled from the mean mantle by taking exclusively into account the principal moments of inertia of mantle and crust C_m and A_m. Numerical values for all these constants are summarized in Table 1. Note that several authors proposed expressions for the EAM functions with slightly different coefficients than those used here; see *Gross* [2009] for review.

[17] Geophysical EAM functions have been calculated from atmospheric and oceanic data sampled four times a day concurrent with ECMWF analysis times starting at 00:00 UTC. By assuming an inverse barometric response of the oceans (IB), atmospheric mass anomalies in oceanic regions have been replaced by the mean atmospheric pressure averaged over the global ocean areas. Consequently, ocean bottom pressure anomalies that are caused by the mass of the water column and the overlying atmosphere have been reduced by the same mean atmospheric pressure in order to represent the deviation of the oceans from the IB assumption only. Since the land surface model LSDM is integrated with a 24 h time step, hydrospheric angular momentum functions (HAM) are provided with daily

Table 1. Numerical Values Applied for the Calculation of the Effective Angular Momentum Functions

Parameter	Value	Definition
r	6371 km	Earth mean radius
ω	7.292115×10^{-5} rad^{-1}	Earth mean angular velocity
K_2	0.295	rotational Love number of degree 2
k_s	0.938	secular (fluid limit) Love number
k_l	−0.301	load Love number
C_m	7.1237×10^{37} kg m^2	(3,3) component mantle tensor of inertia
A_m	7.0999×10^{37} kg m^2	(1,1) component mantle tensor of inertia

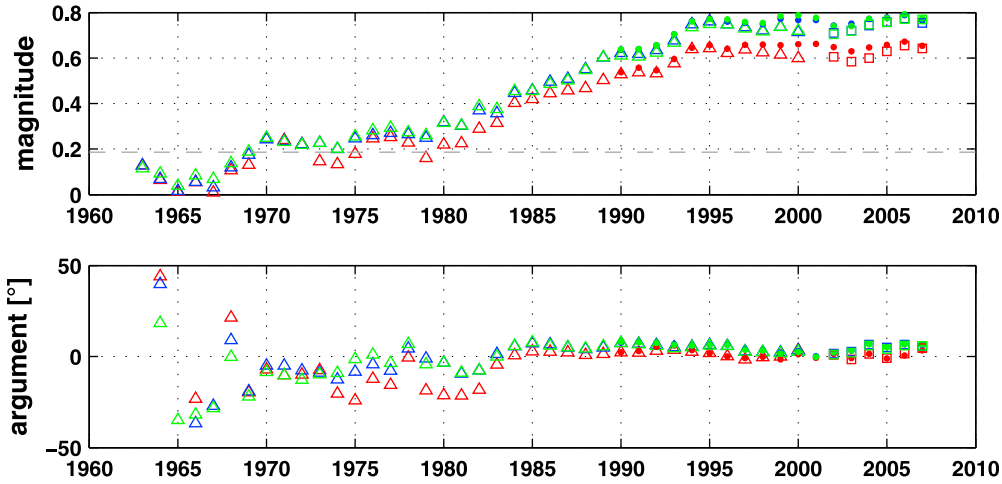

Figure 3. Complex correlations calculated for 3 year width sliding window values from deseasoned and detrended geophysical excitation functions of the atmosphere (red), the sum of atmosphere and ocean (blue), as well as the sum of atmosphere, ocean, and continental hydrosphere (green) with geodetic excitation functions based on EOP-C04, as derived from three different simulations based on ERA40 (triangles), ERA Interim (dots), and operational ECMWF data (squares). The 95% significance level of correlation is indicated by the dashed line.

resolution. AAM and OAM used in this study are therefore averaged to daily values as well.

5. Comparison With Geodetic EAM Functions

[18] The coordinates of the celestial intermediate pole (CIP) reported by the IERS within the EOP C04 series [*Bizouard and Gambis*, 2009] from 1962 onward were transformed to corresponding geodetic excitation functions by applying the deconvolution method of *Wilson and Vicente* [1990]. A complex Chandler frequency with period T_{cw} = 433 days and damping Q = 179 has been applied. Long-term variability and trends have been removed from both geodetic and geophysical EAM functions by a best fitting cubic polynomial. Additionally, complex sinusoids of annual, semiannual, and ter-annual period have been estimated and removed.

[19] Coincidence between these (residual) geodetic and geophysical excitation functions is evaluated by means of complex correlations expressed in magnitude and phase argument. In order to both exclude periods longer than a few years and to demonstrate improvements over time, complex correlations have been calculated for sliding windows of 3 years width that have been individually detrended prior to the correlation analysis (Figure 3). Average decorrelation times for the EAM series have been estimated with 10 days, leading to 110 independent samples within a 3 years period. Therefore, correlation magnitudes larger than 0.19 have been found to be significant with 95% confidence.

[20] Correlation magnitudes well below the significance level and broadly scattered phase arguments are apparent in the 1960s, where both atmospheric model data and polar motion observations were less accurate on daily time scales. Correlations improve slightly after 1970 and more rapidly from 1980 onward, where VLBI observations started to provide precise estimates of polar motion and the first operational meteorologic satellites provided globally homogeneous observations for the reanalysis. Correlations are additionally enhanced by considering signals form oceans and the continental hydrosphere in addition to the atmosphere, reaching correlation magnitudes of more than 0.7 in the most recent decade. However, improvements are not large enough for being significant with 95% confidence. Another gradual and consequently not significant improvement in complex correlation is obtained by considering EAM functions based on the more recent ERA Interim reanalysis. With positive impacts of ocean and continental hydrosphere still apparent, EAM functions derived from ERA Interim yield slightly better correlations than ERA-40 and even the operational ECMWF data for every single 3 year time window considered. Therefore, ERA Interim EAM functions will be used throughout the remainder of this study to analyze excitations of the seasonal wobbles in more detail.

5.1. Excitation of the Seasonal Wobbles

[21] ERA Interim-based EAM functions of both mass and motion terms from atmosphere, ocean, and continental hydrosphere are analyzed with respect to their contribution to the excitation of the annual wobble of the Earth and its higher harmonics. Error estimates provided are the 1σ formal uncertainties based on the standard deviations of the postfit residuals; phases refer to 1 January 1989, 00:00 UTC (Table 2). Prograde annual motions (Figure 4) are dominated by atmospheric pressure contributions causing amplitudes of 17 mas, which is slightly higher than in the NCEP reanalysis data set [*Gross et al.*, 2003]. The oceanic contributions for both mass and motion terms are largely consistent in amplitude and phase with earlier estimates from the ECCO ocean model [*Gross et al.*, 2003]. Continental contributions amount to 4 mas, which is slightly lower and about one month earlier when compared to the LDAS results [*Chen and Wilson*, 2005]. In the retrograde annual component, atmospheric surface pressure variations

Table 2. Excitation of the Annual Wobble due to Both Mass and Motion Term Contributions From Atmosphere, Oceans, and Continental Hydrosphere

Process	Prograde		Retrograde	
	Amplitude (mas)	Phase (deg)	Amplitude (mas)	Phase (deg)
AAM only motion	2.21 ± 0.10	−87.6 ± 2.5	0.51 ± 0.10	−125.4 ± 8.7
AAM only mass	16.93 ± 0.13	−100.9 ± 0.4	16.91 ± 0.13	−107.8 ± 0.4
AAM mass + motion	19.08 ± 0.18	−99.4 ± 0.5	17.40 ± 0.18	−108.4 ± 0.6
OAM only motion	2.04 ± 0.06	−39.1 ± 1.1	2.16 ± 0.06	27.4 ± 0.8
OAM only mass	2.99 ± 0.11	−4.4 ± 0.2	1.39 ± 0.11	89.2 ± 4.5
OAM mass + motion	4.81 ± 0.15	−18.4 ± 0.5	3.07 ± 0.15	50.9 ± 2.1
HAM only motion	0.0021 ± 0.0001	134.7 ± 1.0	0.0018 ± 0.0001	−51.5 ± 1.1
HAM only mass	4.43 ± 0.08	32.8 ± 0.6	8.34 ± 0.08	148.9 ± 0.3
HAM mass + motion	4.43 ± 0.08	32.9 ± 0.6	8.34 ± 0.08	148.9 ± 0.3
AAM + OAM only motion	3.87 ± 0.13	−64.4 ± 1.7	1.72 ± 0.13	19.6 ± 1.4
AAM + OAM only mass	16.86 ± 0.17	−90.7 ± 0.6	15.59 ± 0.17	−109.3 ± 0.6
AAM + OAM mass + motion	20.40 ± 0.23	−85.9 ± 0.7	14.57 ± 0.23	−104.1 ± 0.9
AAM + OAM + HAM only motion	3.87 ± 0.13	−64.4 ± 1.7	1.72 ± 0.13	19.6 ± 1.4
AAM + OAM + HAM only mass	14.87 ± 0.18	−76.4 ± 0.7	16.11 ± 0.18	−139.8 ± 0.4
AAM + OAM + HAM mass + motion	18.68 ± 0.25	−73.9 ± 0.7	14.51 ± 0.25	−137.4 ± 0.7
Observations	14.47 ± 0.29	−63.7 ± 1.0	8.70 ± 0.29	−130.1 ± 1.4

are again the most dominant single contribution with an amplitude of 17 mas. Continental water storage anomalies cause with 8 mas a slightly higher amplitude and well matching phase when compared to LDAS. Retrograde annual ocean bottom pressure contributions are found to be much smaller than the corresponding motion terms, which is in contrast to the results of *Gross et al.* [2003].

[22] Semiannual excitations are still dominated by atmospheric pressure distributions, although the relative importance of winds and ocean currents has been increased. The prograde atmospheric mass term has been estimated with 2.3 mas, which is slightly lower than the corresponding NCEP result. The retrograde term is also dominated by atmospheric pressure with 4.4 mas, accompanied by 0.9 and 1.3 mas induced by winds and ocean currents, respectively. While the current term is comparable in amplitude and phase with ECCO, the wind term has been almost doubled with respect to NCEP. Terrestrial contributions are well below 1 mas for both components. Since ter-annual variations are small in both geodetic and geophysical excitation functions, results depend heavily on the time-interval considered. Both atmospheric and oceanic mass terms as well as winds cause

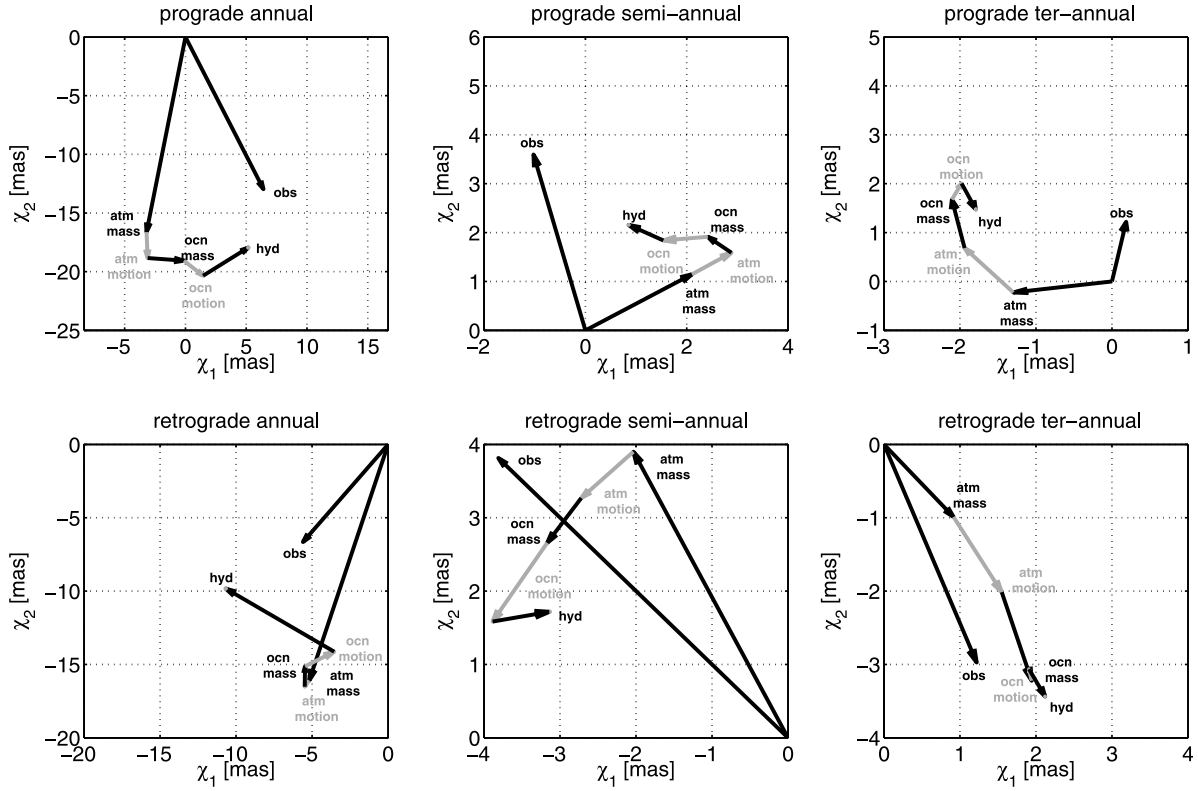

Figure 4. Phasor diagram of prograde and retrograde contributions to the annual, semiannual, and ter-annual wobble derived from simulations based on ERA Interim.

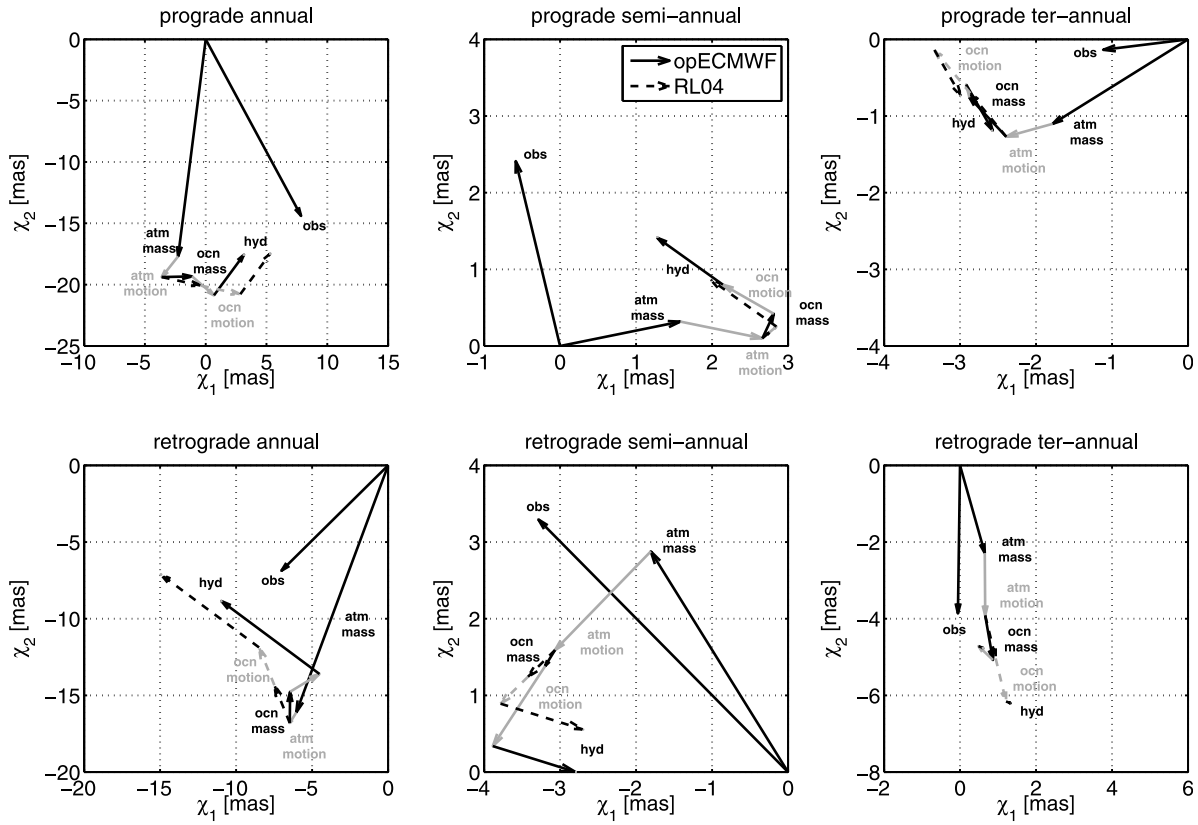

Figure 5. Phasor diagram of prograde and retrograde contributions to the annual, semiannual, and ter-annual wobble derived from operational ECMWF data for OMCT simulations with time variable ocean mass (solid lines; this paper) and ocean mass held constant at every time step (dashed lines [*Dobslaw and Thomas*, 2007]).

prograde and retrograde excitations with about 1 mas amplitude, while ocean currents and continental water storage variations contribute only minor excitation energy to the ter-annual wobble.

[23] Since LSDM also provides estimates of continental water flow velocities in rivers and aquifers, continental motion terms have been calculated in addition to the mass term contributions from terrestrial water storage variations. However, relative angular momentum contributions are three orders of magnitude smaller than the corresponding mass terms [see *Walter*, 2008, for details], leading to annual wobble excitations of about 2 μas (Table 2), and even smaller values for the semiannual and ter-annual wobble excitations.

5.2. Impact of Mass Conservation

[24] In order to evaluate the effect of enforcing mass conservation within the atmosphere, ocean, and continental hydrosphere system on seasonal polar motion, geophysical EAM functions derived from operational ECMWF analyses and corresponding LSDM and OMCT simulations are compared to EAM functions that have been derived from an OMCT simulation with ocean mass held constant at every time step. This model configuration has been previously used to provide the ocean component of the atmosphere-ocean dealiasing product AOD1B RL04 prepared for the satellite gravimetry mission GRACE [*Flechtner*, 2007; *Dobslaw and Thomas*, 2007]. For the annual wobble, amplitudes of the prograde and retrograde ocean mass excitations of the time-variable ocean mass simulation are reduced by 0.8 and 0.6 mas, respectively, when compared to the OMCT version with constant ocean mass (Figure 5). Gradual changes of 0.2 mas in amplitude additionally occur on the semiannual period, while almost no impact of total ocean mass variability on the ter-annual wobble excitation has been identified. Although changes appear substantial for individual excitation components, the overall discrepancy between geodetic and geophysical EAM functions is still too large to unequivocally demonstrate the benefit of considering total ocean mass changes on explaining seasonal polar motion excitation, indicating that errors inherent in the model results of atmosphere, ocean, and continental hydrosphere are, together with dynamical processes still not considered for in the modeling approach, responsible for the nonclosure of the excitation budget on seasonal time scales.

6. Regional Contributions

[25] In order to demonstrate the richness of processes responsible for the excitation of the seasonal wobbles as predicted by the numerical models, regional excitation contributions are described by the sum of the best fitting sinusoids of annual, semiannual, and ter-annual period for every 1° × 1° grid box. Contributions are integrated over latitude bands and displayed in Hovmoeller diagrams over the course of a year (Figures 6 and 7). The data have been

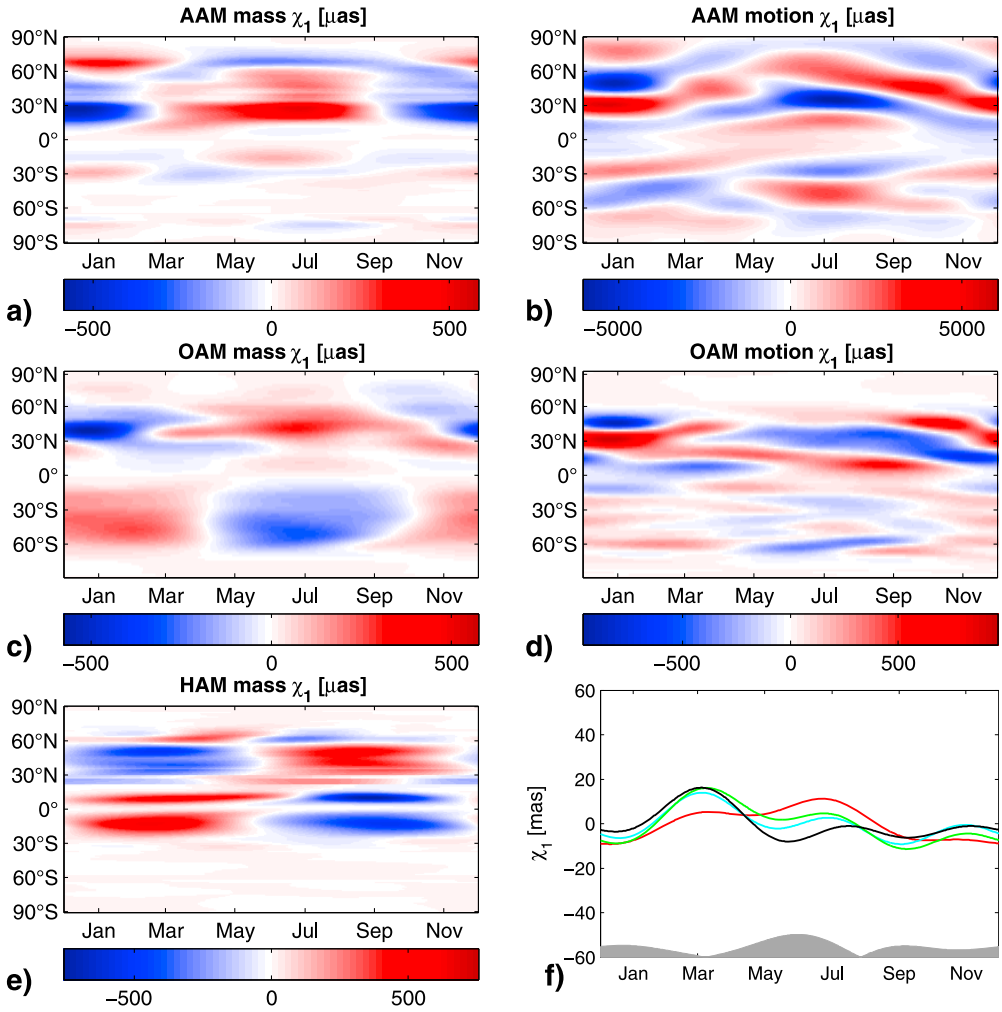

Figure 6. Zonally integrated contributions to χ_1 from (a) atmospheric surface pressure anomalies, (b) atmospheric winds, (c) ocean bottom pressure changes, (d) ocean currents, and (e) continental hydrospheric mass anomalies. (f) Globally integrated contributions from atmosphere (red), the sum of atmosphere and ocean (blue), as well as the sum of atmosphere, ocean, and continental hydrosphere (green) are contrasted against observations (black). Absolute values of differences between observations and simulated effects of atmosphere, oceans, and continental hydrosphere are depicted in gray columns at the bottom.

smoothed in meridional direction with a 5° boxcar filter in order to focus on large-scale variability only.

[26] For the atmospheric mass component, high pressure over Eurasia during the northern hemispheric winter cause negative contributions to both excitation components (Figures 6a and 7a). High pressure over Australia during the southern hemispheric winter contributes negatively to χ_1 and positively to χ_2, but its effect is almost fully compensated by comparable surface pressure anomalies over South America, leading to small net-contributions of the Southern Hemisphere only. Since large-scale wind patterns are aligned zonally, contributions are in particular high when individual latitude bands are considered, although most of the signals compensate each other when integrated globally (Figures 6b and 7b). Prominent excitations originate from the North Pacific area, where enhanced winter-time jet stream velocities cause positive contributions to χ_1. Comparable signals are also apparent in the Southern Hemisphere leeward of Australia during July and August, although magnitudes are lower compared to the Northern Hemisphere due to the smaller land extent.

[27] Terrestrial water storage contributions are comparable to excitations caused by atmospheric pressure (Figures 6e and 7e). Negative (positive) excitations in χ_1 (χ_2) of subpolar and moderate northern latitudes peak in March, concurrent with the onset of the annual melt season. During Northern Hemisphere's fall, the rain season starts in the tropics of the Southern Hemisphere, leading to accumulation of mass in Amazon, Congo, and other basins which compensates for snow accumulation elsewhere and produces a small net impact of the continental hydrosphere on χ_1 only. Higher polar motion excitation contributions for the χ_2 component are due to the combined effects of North American snow deposition and the dry season in the southeast Asian monsoon areas that both cause positive effects on the polar motion excitation during the first half of the year.

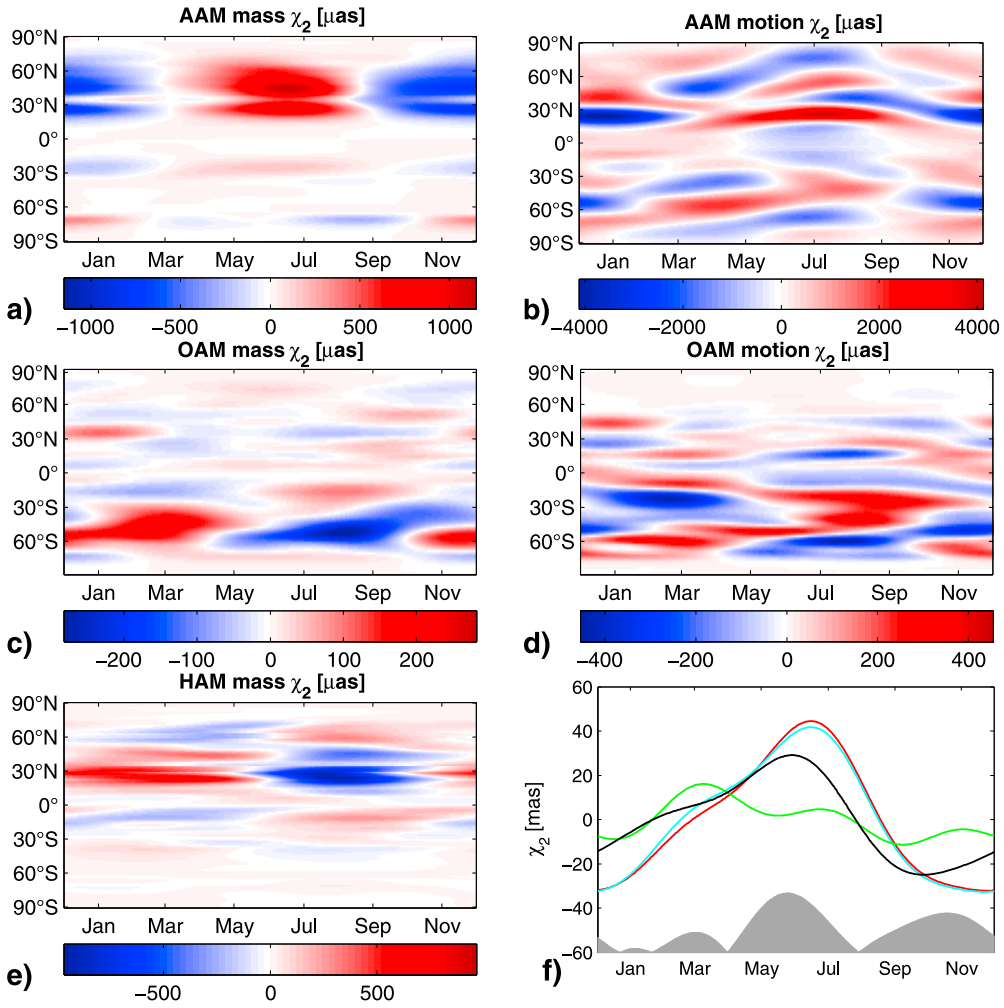

Figure 7. Same as in Figure 6, but for $\chi_2$contribution.

[28] Excitations caused by ocean bottom pressure changes (Figures 6c and 7c) are highest in the Southern Ocean, where large mass redistributions take place within the turbulent flow of the Antarctic Circumpolar Current (ACC). Positive excitations in both components between November and March are related to positive mass anomalies in the South Atlantic (χ_1) and the Indian Ocean (χ_2). Contributions from the Northern Hemisphere are much smaller and almost entirely confined to the North Pacific Ocean, where positive mass anomalies during the second half of the year have a positive impact on χ_1. For the motion term, currents primarily located in the Indian Ocean and the western North Pacific vary rapidly in response to fluctuating wind patterns (Figures 6d and 7d), although local magnitudes remain much lower when compared to the wind contributions. Generally, local ocean mass anomalies are weaker than corresponding surface pressure variations or changes in continental water storage, but since they extend over much larger regions, their zonally integrated contributions are, at least for the χ_1 component, of comparable magnitude with atmosphere and the continental hydrosphere.

[29] Finally, geophysical EAM functions of all subsystems are integrated globally and compared to the corresponding geodetic excitation functions (Figures 6f and 7f). Although correspondence is generally improved when oceanic and continental effects are added to the atmospheric contributions, substantial discrepancies remain for χ_1 in June, where the excitation minimum is simulated weaker and earlier. For χ_2, the maximum excitation in June and the following minimum in September are considerably underestimated by the model combination. By recognizing the comparable magnitudes of regional mass contributions from atmosphere, ocean, and continental hydrosphere, it becomes clear that these discrepancies might be caused by any of the subsystems considered here.

7. Summary and Conclusions

[30] Global atmospheric data from the ECMWF have been used to force the land surface model LSDM and the ocean model OMCT, to provide estimates of mass distributions and mass movements of atmosphere, ocean, and continental hydrosphere. Mass exchanges among the subsystems are realized by means of freshwater fluxes, causing the total ocean mass to vary predominantly annually whereas the sum of all masses contained in atmosphere,

ocean and continental hydrosphere is held constant. The model output allowed the derivation of geophysical effective angular momentum functions over more than four decades with at least daily resolution. Correlations with geodetic excitation functions derived from pole coordinate observations are significantly improved during the years, with correlation magnitudes exceeding 0.7 in the most recent decade that are achieved when atmospheric, oceanic, and hydrospheric contributions are considered together.

[31] Based on 20 years of ERA Interim simulations, the excitation of the seasonal wobbles has been re-assessed. Although the contributions of individual subsystems sometimes differ substantially from previously reported results, as, e.g., the ocean bottom pressure contribution to the retrograde annual component, discrepancies of the summarized effects of atmosphere, ocean and continental hydrosphere are on a comparable level as achieved before with alternative numerical models. Relative angular momentum contributions due to river flow have been found to be three orders of magnitude smaller than corresponding effects of continental water storage changes, allowing to neglect continental motion terms while studying variations in the Earth's rotation. The contribution of a time variable ocean mass due to mass re-distributions in the Earth's system was estimated to be 0.8 mas in the annual prograde, and 0.6 mas in the retrograde component.

[32] Although seasonal variations in total ocean mass are largely consistent with observations from GRACE, differences between geodetic and geophysical excitations of the seasonal wobbles are not substantially reduced when these contributions are included, indicating that the closure of the seasonal excitation budget is still inhibited by remaining errors in all subsystems. Apart from atmospheric motion terms, that account for up to 5 mas of selected bands in moderate latitudes due to zonally aligned wind patterns, regional contributions of atmosphere, ocean, and continental hydrosphere are of comparable magnitude. Therefore, mass distributions in all subsystems need to be equitably evaluated in order to identify model errors responsible for the misclosure of the excitation budget. Monthly mean mass anomalies obtained from the satellite gravity mission GRACE are well suited to serve as a reference for the mass terms [see, e.g., *Nastula et al.*, 2007], while major improvements for global wind observations are only expected from the satellite-based Doppler wind lidar instrument aboard the ESA mission ADM-Aeolus scheduled for launch in 2011.

[33] **Acknowledgments.** We thank Johannes Wünsch for helpful insights into Earth rotation observations and Claudia Walter for her contributions toward the development of the LSDM. Deutscher Wetterdienst, Offenbach, Germany, and the European Centre for Medium-Range Weather Forecasts are acknowledged for providing data from ECMWF's operational model. Numerical simulations were performed at Deutsches Klimarechenzentrum, Hamburg, Germany. This work has been supported by Deutsche Forschungsgemeinschaft within the research unit Earth Rotation and Global Dynamic Processes under grant TH864/7-1.

References

Andersson, E., et al. (2005), Assimilation and modelling of the atmospheric hydrological cycle in the ECMWF forecasting system, *Bull. Am. Meteorol. Soc.*, *86*, 387–401, doi:10.1175/BAMS-86-3-387.

Barnes, R. T. H., R. Hide, A. A. White, and C. A. Wilson (1983), Atmospheric angular momentum fluctuations, length-of-day changes and polar motion, *Proc. R. Soc. London A*, *387*, 31–73, doi:10.1098/rspa.1983.0050.

Bizouard, C., and D. Gambis (2009), The combined solution C04 for Earth orientation parameters recent improvements, in *Geodetic Reference Frames: IAG Symposium Munich, Germany, 9–14 October 2006*, *Int. Assoc. Geod. Symp.*, vol. 134, edited by H. Drewes, pp. 265–270, doi:10.1007/978-3-642-00860-3_41, Springer, New York.

Bizouard, C., and L. Seoane (2010), Atmospheric and oceanic forcing of rapid polar motion, *J. Geod.*, *84*, 19–30, doi:10.1007/s00190-009-0341-2.

Brzeziński, A., J. Nastula, and B. Kolaczek (2009), Seasonal excitation of polar motion estimated from recent geophysical models and observations, *J. Geodyn.*, *48*, 235–240, doi:10.1016/j.jog.2009.09.021.

Chambers, D. P., J. Wahr, and R. S. Nerem (2004), Preliminary observations of global ocean mass variations with GRACE, *Geophys. Res. Lett.*, *31*, L13310, doi:10.1029/2004GL020461.

Chen, J. L., and C. R. Wilson (2005), Hydrological excitations of polar motion, 1993–2002, *Geophys. J. Int.*, *160*, 833–839, doi:10.1111/j.1365-246X.2005.02522.x.

Clarke, P. J., D. A. Lavallee, G. Blewitt, T. M. van Dam, and J. M. Wahr (2005), Effect of gravitational consistency and mass conservation on seasonal surface mass loading models, *Geophys. Res. Lett.*, *32*, L08306, doi:10.1029/2005GL022441.

Dill, R. (2009), Hydrological model LSDM for operational Earth rotation and gravity field variations, *Sci. Tech. Rep.*, 08/09, Deutsches GeoForschungsZentrum, Potsdam, Germany.

Dobslaw, H., and M. Thomas (2007), Simulation and observation of global ocean mass anomalies, *J. Geophys. Res.*, *112*, C05040, doi:10.1029/2006JC004035.

Drijfhout, S., C. Heinze, M. Latif, and E. Maier-Reimer (1996), Mean circulation and internal variability in an ocean primitive equation model, *J. Phys. Oceanogr.*, *26*, 559–580, doi:10.1175/1520-0485(1996)026<0559:MCAIVI>2.0.CO;2.

Flechtner, F. (2007), AOD1B product description document, GRACE327–750, rev. 3.1, 43 pp., GeoForschungsZentrum, Potsdam, Germany.

Graversen, R. G., E. Källen, M. Tjernström, and H. Körnich (2007), Atmospheric mass-transport inconsistencies in the ERA-40 reanalysis, *Q. J. Meteorol. Soc.*, *133*, 673–680, doi:10.1002/qj.35.

Greatbatch, R. J. (1994), A note on the representation of steric sea level in models that conserve volume rather than mass, *J. Geophys. Res.*, *99*(C6), 12,767–12,771, doi:10.1029/94JC00847.

Gross, R. M. (2009), Earth rotation variations—Long period, in *Treatise on Geophysics–Geodesy*, edited by T. Herring, pp. 239–294, Elsevier, Amsterdam, Netherlands.

Gross, R. M., I. Fukumori, and D. Menemenlis (2003), Atmospheric and oceanic excitation of the Earth's wobbles during 1980–2000, *J. Geophys. Res.*, *108*(B8), 2370, doi:10.1029/2002JB002143.

Hagemann, S. (1998), *Entwicklung einer Parametrisierung des lateralen Abflusses für Landflächen auf der globalen Skala*, Examensarbeit *52*, Max-Planck-Inst. für Meteorol, Hamburg, Germany.

Hagemann, S., and L. Dümenil (1998), A parametrization of the lateral waterflow for the global scale, *Clim. Dyn.*, *14*, 17–31, doi:10.1007/s003820050205.

Hagemann, S., K. Arpe, and L. Bengtsson (2005), *Validation of the hydrological cycle of ERA-40*, *ERA-40 Proj. Ser. 24*, Eur. Cent. for Medium-Range Weather Forecasts, Reading, U. K.

Kuehne, J., and C. Wilson (1991), Terrestrial water storage and polar motion, *J. Geophys. Res.*, *96*(B3), 4337–4345, doi:10.1029/90JB02573.

Nastula, J., R. M. Ponte, and D. A. Salstein (2007), Comparison of polar motion excitation series derived from GRACE and from analyses of geophysical fluids, *Geophys. Res. Lett.*, *34*, L11306, doi:10.1029/2006GL028983.

Nastula, J., D. Salstein, and B. Kolaczek (2009), Patterns of atmospheric excitation functions of polar motion from high-resolution regional sectors, *J. Geophys. Res.*, *114*, B04407, doi:10.1029/2008JB005605.

Ponte, R. M., D. Stammer, and J. Marshall (1998), Oceanic signals in observed motions of the Earth's pole of rotation, *Nature*, *391*, 476–479, doi:10.1038/35126.

Randel, W. J., et al. (2009), An update of observed stratospheric temperature trends, *J. Geophys. Res.*, *114*, D02107, doi:10.1029/2008JD010421.

Rosen, R. D., and D. A. Salstein (1983), Variations in atmospheric angular momentum on global and regional scales and the length of day, *J. Geophys. Res.*, *88*(C9), 5451–5470, doi:10.1029/JC088iC09p05451.

Thomas, M. (2002), Ocean induced variations of Earth's rotation—Results from a simultaneous model of global circulation and tides, Ph.D. dissertation, 129 pp., Univ. of Hamburg, Hamburg, Germany.

Uppala, S. M., et al. (2005), The ERA-40 reanalysis, *Q. J. Meteorol. Soc.*, *131*, 2961–3012, doi:10.1256/qj.04.176.

Uppala, S., D. Dee, S. Kobayashi, P. Berrisford, and A. Simmons (2008), Toward a climate data assimilation system: Status update of ERA Interim, *ECMWF Newsl.*, *115*, 12–18.

Walter, C. (2008), Simulation of hydrospheric mass variations and their impact on the Earth's rotation, Ph.D. dissertation, 196 pp., Inst. für Planet. Geod., Tech. Univ. Dresden, Dresden, Germany.

Wilson, C., and R. Vicente (1990), Maximum likelihood estimates of polar motion parameters, in *Variations in Earth Rotation*, *Geophys. Monogr. Ser.*, 59, edited by D. D. McCarthy and W. E. Carter, pp. 151–155, AGU, Washington, D. C.

Wolff, J. O., E. Maier-Reimer, and S. Legutke (1996), The Hamburg Ocean Primitive Equation Model HOPE, *Tech. Rep. 13*, Dtsch. Klimarechenzentrum, Hamburg, Germany.

A. Brzeziński, Faculty of Geodesy and Cartography, Warsaw University of Technology, Bartycka 18A, Warsaw, 00-716, Poland. (alek@cbk.waw.pl)

R. Dill, H. Dobslaw, A. Grötzsch, and M. Thomas, Section 1.3: Earth System Modeling, Deutsches GeoForschungsZentrum, Telegrafenberg, D-14473 Potsdam, Germany. (dill@gfz-potsdam.de; dobslaw@gfz-potsdam.de; groetz@gfz-potsdam.de; mthomas@gfz-potsdam.de)